European Journal of Medicinal Chemistry 124 (2016) 350–360

Contents lists available at ScienceDirect

European Journal of Medicinal Chemistry

journal homepage: http://www.elsevier.com/locate/ejmech

Short communication

# Design and synthesis of isatin/triazole conjugates that induce apoptosis and inhibit migration of MGC-803 cells

Bin Yu[*, 1], Sai-Qi Wang [1], Ping-Ping Qi, Dong-Xiao Yang, Kai Tang, Hong-Min Liu[**]

*School of Pharmaceutical Sciences & Collaborative Innovation Center of New Drug Research and Safety Evaluation, Zhengzhou University, Zhengzhou 450001, China*

ARTICLE INFO

*Article history:*
Received 20 March 2016
Received in revised form
25 August 2016
Accepted 26 August 2016
Available online 28 August 2016

*Keywords:*
Isatin
Triazole
Cytotoxicity
Apoptosis
Migration inhibition
LSD1 inactivation

ABSTRACT

A series of new isatin/triazole conjugates were designed based on the hypothesis that the ester-linked compounds could be enzymatically hydrolyzed by cellular esterases inside the cells. These compounds showed moderate to good growth inhibition toward the tested cancer cells, exerted selective inhibition toward MGC-803 cells and were less toxic to normal cells HL-7702 and GES-1. Of these compounds, compound **5a** showed the best inhibitory activity against MGC-803 cells ($IC_{50}$ = 9.78 μM), induced apoptosis through multiple mechanisms, as well as inhibited migration of MGC-803 cells.



## 1. Introduction

Isatin, a well-known natural indole derivative found in many plants, has also been observed as a metabolite of adrenaline in human bodies [1]. Recent studies indicated that isatin itself is capable of inhibiting growth of SH-SY5Y cells and inducing apoptosis via the intrinsic apoptotic pathway [2,3]. Isatin-based structural modifications have been highly pursued in last decades because isatin derivatives have been found to possess diverse and promising biological activities, and some of these isatin derivatives have shown therapeutical effects in preclinical investigations [4–9]. Representative examples are SAR405835 [10], CFI-400945 [11], and KAE609 [12] (Fig. 1), which are currently undergoing clinical assessment for the treatment of cancer and malaria, respectively. In addition to the biological functions, isatin and its derivatives have also found synthetic utilities in the construction of spirooxindole frameworks due to the high reactivity of C3 carbonyl group [13–15]. On the other hand, the 1,2,3-triazole group has proven to be metabolically stable and able to decrease the aqueous solubility and therefore has been extensively used in the design of bioactive molecules [16–18].

As part of our efforts toward the identification of potent anticancer agents, we previously introduced the isatin motif to the steroid nucleus, generating a large library of structurally new steroidal oxindoles with good antiproliferative activity [19–22]. Intriguingly, a series of steroid/isatin conjugates were identified as the first steroid-based lysine specific demethylase 1 (LSD1) inhibitors, which inactivated LSD1 at low micromolar levels [23]. The shortlisted compound **I** (Fig. 2) was found to be able to inhibit growth of cancer cells and induce apoptosis. The carboxylic ester group is believed to be able to be hydrolyzed by cellular esterases inside the cells, giving the free carboxylic acid and alcohol. The characteristics of the ester group make it widely used in the design of prodrugs [24–26] and fluorescent probes such as the DCFH-DA for cellular ROS detection [27]. Evidently, both parts of compound **I** are linked through the ester group and therefore could be potentially enzymatically hydrolyzed to afford the DHEA and another fragment (the isatin/triazole conjugate). It is well-known that DHEA inhibits growth of cancer cells through multiple mechanisms [28–32]. Therefore, the question remains whether the compound **I** exerted the good cytotoxicity alone or through the synergistic effects of both components. The hypothesis promoted us to investigate the anticancer potential of the isatin/triazole fragment by varying the R group (Fig. 2). We herein report the

* Corresponding author.
** Corresponding author.
*E-mail addresses:* zzuyubin@hotmail.com (B. Yu), liuhm@zzu.edu.cn (H.-M. Liu).
[1] Bin Yu and Sai-Qi Wang contributed equally to this work.

http://dx.doi.org/10.1016/j.ejmech.2016.08.065
0223-5234/

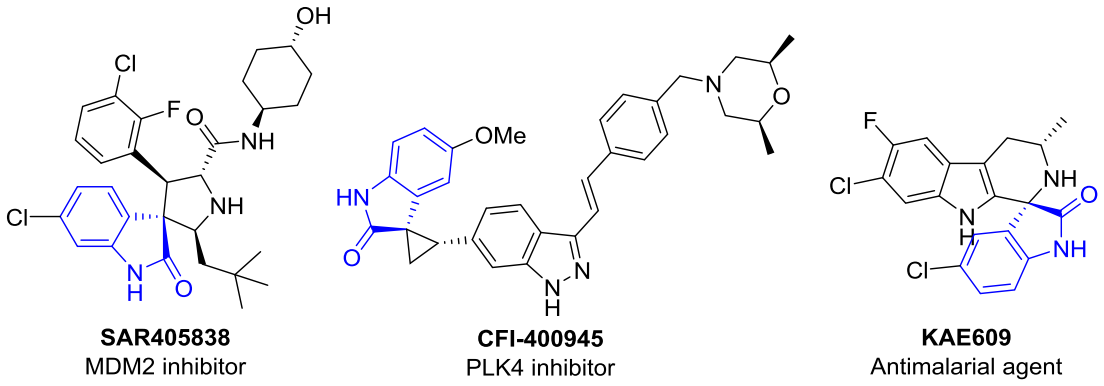


**Fig. 1.** Representative examples of isatin-derived oxindole derivatives.

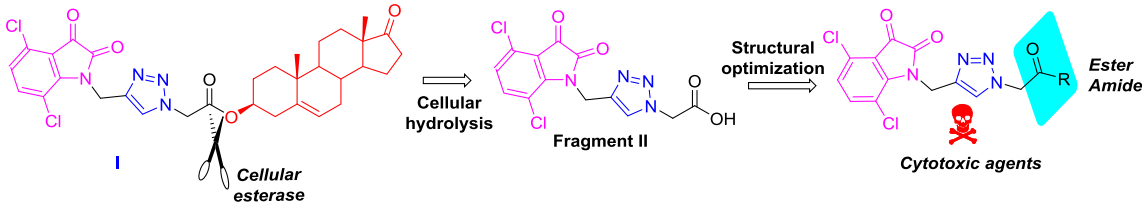


**Fig. 2.** Identification of isatin/triazole conjugates with anticancer potential.

cytotoxicity of the isatin/triazole conjugates against several cancer cells and the possible modes of action, hoping to provide a basis for the development of isatin-based anticancer agents.

## 2. Results and discussion

### 2.1. Chemistry

The synthesis of compounds **5a**–**h** is operationally simple using the Cu-catalyzed click chemistry as the key step (Scheme 1). 4, 7-Dichloroisatin **1** reacted with propargyl bromide in the presence of $K_2CO_3$ gave compound **2**, which then reacted with azido compounds **4a**–**g**, affording compounds **5a**–**g**. Compounds **4a**–**g** were synthesized from compounds **3a**–**g** and sodium azide through the nucleophilic substitution. Compound **2** and compounds **4a**–**g** were then subjected to the Cu-catalyzed Click reactions, affording compounds **5a**–**g**. Deprotection of compound **5g** in the presence of TFA generated compound **5h** bearing a terminal amine salt.

### 2.2. Cytotoxicity evaluation

With these compounds in hand, we next tested their

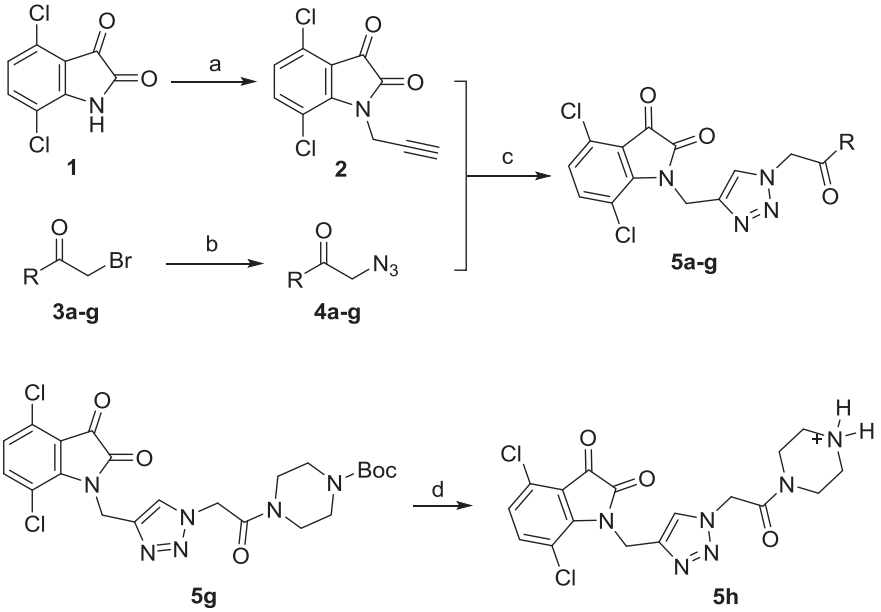


**Scheme 1.** Synthesis of compounds **5a**–**h**. Reagents and conditions: (a) Propargyl bromide, $K_2CO_3$, DMF, rt; (b) $NaN_3$, DMSO, rt-50 °C; (c) Sodium ascorbate, $CuSO_4 \cdot 5H_2O$, THF/$H_2O$ (1/1), rt; (d) TFA, DCM, rt.

cytotoxicity against several cancer cell lines (TE-1, MCF-7, SW780, and MGC-803) using the CCK-8 assay. Also, the cytotoxic evaluation of compounds **5a**–**g** against normal cells HL-7702 and GES-1 was carried out to explore the toxicity and selectivity. In the assay, the well-known anticancer drug 5-flurouracil (5-FU) was used as the control. However, we failed to test the inhibitory effect of compound **5h** toward the tested cancer cell lines because of its poor solubility observed.

As shown in Table 1, compounds **5a**–**g** exhibited moderate to good inhibitory effect toward the tested cancer cell lines. Interestingly, compared to compounds **5b**–**g** with different terminal carboxylic amide groups, compound **5a** bearing an enzymatically hydrolyzable ester group showed the best inhibition against all the tested cancer cell lines with the $IC_{50}$ values less than 26 μM, possibly suggesting that a terminal carboxylic acid group for this series of compounds is beneficial for the activity. This finding gives us directions for further structural modifications. Compound **5a** displayed good inhibition against TE-1 and MGC-803 with the $IC_{50}$ values of 14.22 and 9.78 μM, respectively, comparable to that of 5-FU. For compounds **5a**–**g**, the moderate to weak inhibitory effect was observed toward TE-1, MCF-7 and SW780 with the $IC_{50}$ values ranging from 25 to >128 μM. It should be noted that compound **5f** with a terminal morpholine group showed significantly decreased inhibition against all the tested cancer cells, compared to the structurally similar compound **5d**. The underlying mechanism remains unknown. More intriguingly, compounds **5a**–**g** were more sensitive to MGC-803 cells, indicating that this series of compounds may exert the inhibitory effect by targeting overexpressed cancer-related proteins in MGC-803 cells. It has been proved that LSD1 is overexpressed in MGC-803 cells, and we have successfully designed three series of selective LSD1 inhibitors, which potently inhibited growth of MGC-803 cells *in vitro* and *in vivo* [33–35]. However, whether the selective inhibition of compounds **5a**–**g** toward MGC-803 cells is due to the LSD inactivation remains unclear and needs to be investigated further, although the structurally similar compound **I** (Fig. 2) inhibits LSD1 at low micromolar levels. Furthermore, compounds **5a**–**g** were less sensitive to normal cells over cancer cells, showing certain selectivity between normal and cancerous cells. Also, compounds **5a**–**g** were less toxic toward normal cells than 5-FU. The low toxicity and selectivity warrant their further development for identifying more potent isatin-based anticancer agents.

### 2.3. *In silico* prediction of drug-like properties of compounds ***5a*–*h***

Molecular properties of designed compounds **5a**–**h** were calculated using the free molecular calculation services provided by Molinspiration (http://www.molinspiration.com). As shown in Table 2, compounds **5a**–**h** showed favorable drug-like properties that are in line with the Lipinski's rule of five [36].

### 2.4. *Morphological changes of MGC-803 cells induced by compound **5a***

Morphological changes of cancer cells are always associated with the growth inhibition induced by cytotoxic agents [37,38]. Inspired by the good inhibition of compound **5a** against MGC-803 cells, we then investigated whether compound **5a** was able to induce morphological changes. After being incubated with **5a** for 24 h at different concentrations (0, 5, 10, 20 μM), the morphological changes of MGC-803 cells were recorded using an inverted microscope. As shown in Fig. 3A, significant changes of cell morphology such as rounding up and cell debris were observed, especially at high concentrations. After staining with Hoechst 33258, remarkable nuclear changes including the chromatin condensation, nuclear fragmentation and condensation were also

**Table 1**
Preliminary *in vitro* cytotoxicity of compounds **5a**–**h** against the tested cancerous and normal cell lines.

| Compound | R | $IC_{50}$ (μM) | | | | | |
|---|---|---|---|---|---|---|---|
| | | TE-1 | MCF-7 | SW780 | MGC-803 | HL-7702 | GES-1 |
| **5a** |  | 14.22 ± 4.09 | 18.86 ± 0.67 | 25.21 ± 3.65 | **9.78 ± 1.67** | 40.27 ± 10.00 | 35.97 ± 6.32 |
| **5b** |  | 25.19 ± 4.36 | 51.8 ± 2.80 | 93.33 ± 16.56 | **17.40 ± 2.44** | 83.92 ± 12.25 | 47.429 ± 7.32 |
| **5c** |  | 30.61 ± 14.03 | 38.46 ± 4.80 | 26.97 ± 7.97 | **17.48 ± 5.95** | 24.87 ± 4.11 | 24.87 ± 2.00 |
| **5d** |  | 40.62 ± 10.23 | 34.61 ± 6.59 | 29.69 ± 5.08 | **18.67 ± 4.55** | 39.29 ± 7.13 | 50.693 ± 6.32 |
| **5e** |  | 51.60 ± 12.77 | 62.35 ± 4.66 | 48.22 ± 8.90 | **14.75 ± 1.27** | >128 | 88.72 ± 10.73 |
| **5f** |  | 118.93 ± 18.75 | 146.40 ± 36.75 | 112.74 ± 22.10 | **51.70 ± 14.60** | >128 | >128 |
| **5g** |  | 39.25 ± 4.58 | 46.85 ± 5.65 | >128 | **22.04 ± 6.68** | 41.96 ± 10.12 | 84.19 ± 7.83 |
| **5h**[a] |  | – | – | – | – | – | – |
| **5-FU** | – | 17.32 ± 3.98 | 13.19 ± 0.81 | 6.99 ± 2.60 | 10.64 ± 2.96 | 12.85 ± 1.22 | 13.75 ± 3.41 |

[a] The cytotoxicity of compound **5h** was not determined because of its poor solubility in the CCK-8 assay.

**Table 2**
Molecular properties of compounds **5a**–**h.**[a]

| Compound | MW | nviolations | natoms | nON | nOHNH | nrotb | miLogP | TPSA | MV |
|---|---|---|---|---|---|---|---|---|---|
| Desirable value | <**500** | – | – | <**10** | <**5** | ≤**10** | <**5** | <**140** | – |
| **5a** | 437.28 | 0 | 29 | 8 | 0 | 6 | 3.67 | 96.10 | 351.05 |
| **5b** | 436.30 | 0 | 29 | 8 | 1 | 5 | 2.92 | 98.89 | 354.47 |
| **5c** | 430.25 | 0 | 29 | 8 | 1 | 5 | 2.71 | 98.89 | 335.88 |
| **5d** | 422.27 | 0 | 28 | 8 | 0 | 4 | 2.17 | 90.10 | 338.02 |
| **5e** | 408.25 | 0 | 27 | 8 | 0 | 4 | 1.66 | 90.10 | 321.22 |
| **5f** | 424.24 | 0 | 28 | 9 | 0 | 4 | 1.10 | 99.34 | 330.21 |
| **5g** | 523.38 | 2 | 35 | 11 | 0 | 6 | 2.19 | 119.65 | 428.16 |
| **5h** | 424.27 | 0 | 28 | 9 | 2 | 4 | −2.11 | 106.71 | 334.60 |
| **5-FU** | 130.08 | 0 | 9 | 4 | 2 | 0 | −0.59 | 65.72 | 96.91 |

[a] MW: Molecular weight; nviolations: Number of violations; natoms: Number of atoms; nON: Number of hydrogen bond acceptors; nOHNH: Number of hydrogen bond donors; nrotb: Number of rotatable bonds; miLogP: LogP value predicted by Molinspiration; TPSA: Topological polar surface area; MV: Molecular volume.

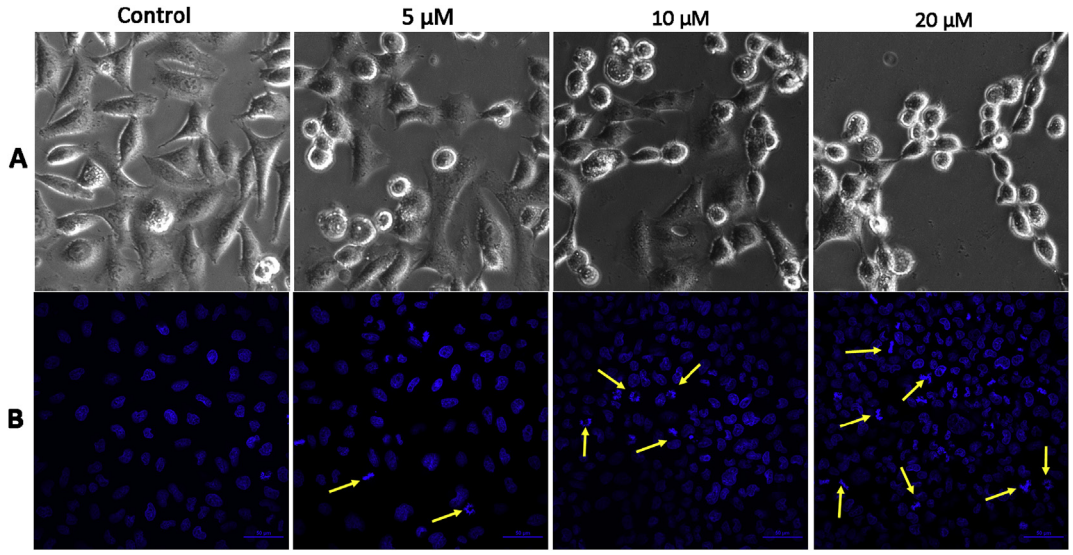


**Fig. 3.** Morphological changes (A) and nuclear degradation (B) of MGC-803 cells induced by compound **5a**. Scale bar is 50 μm.

observed (Fig. 3B).

### 2.5. Cell cycle distribution assay by flow cytometry

Targeting the cell cycle of tumor cells has been recognized as a promising strategy for cancer therapy [39]. In this study, compound **5a** was chosen to investigate the effect of our designed conjugates on the cell cycle of MGC-803 cells. After treating MGC-803 cells with compound **5a** at different concentrations (0, 5, 10, 20 μM) for 24 h, cells were then fixed and stained with PI for flow cytometry analysis. As shown in Fig. 4, compound **5a** concentration-dependently arrested cell cycle at G2/M phase, accompanied with decrease of cells at G0/G1 phase. Specifically, the percentage of cells at G2/M phase for the high concentration group (20 μM) was 32.26%, about 12% higher than that of the control group.

### 2.6. Apoptosis detection by flow cytometry

The effect of compound **5a** on the apoptosis was investigated using the propidium iodide (PI) and Annexin V-FITC biparametric cytofluorimetric analysis. After treatment with different concentrations of compound **5a** (0, 5, 10 and 20 μM) for 24 h, MGC-803 cells were stained with PI and FITC, and then analyzed by the flow cytometry. As illustrated in Fig. 5, compound **5a** induced apoptosis of MGC-803 cells in a concentration-dependent manner, especially the early apoptosis. Specifically, the percentage of apoptotic cells was about 1.3% for the control group. When treated with high concentration (20 μM) of compound **5a**, around 22.5% of apoptosis rate was observed. While the late apoptosis rate of MGC-803 cells was not changed significantly with increasing concentrations.

### 2.7. Measurement of intracellular ROS levels

Studies above showed that compound **5a** can arrest the cell cycle at G2/M phase and induce the apoptosis concentration-dependently. However, the precise mechanisms of action remain unclear. Oliveira et al. reported that *Uncaria tomentosa* extract containing oxindole alkaloids triggered apoptosis of HT29 cells through the ROS-mediated caspase activation and DNA repair [40]. More recently, Shankaraiah and co-workers reported that spirooxindole-derived morpholine-fused-1,2,3-triazoles can increase ROS levels in A549 cells and decrease the mitochondrial membrane potential, finally leading to apoptosis of A549 cells [41]. These studies suggest that isatin-derived compounds could have the potential of increasing cellular ROS levels. From the structural point of view, we reasoned that treatment of MGC-803 cells with the designed isatin/triazole conjugates could also induce cellular ROS production, which then contributed to the apoptosis of cancer cells.

To investigate whether compound **5a** is capable of inducing ROS generation in MGC-803 cells, the DCFH-DA (2,7-

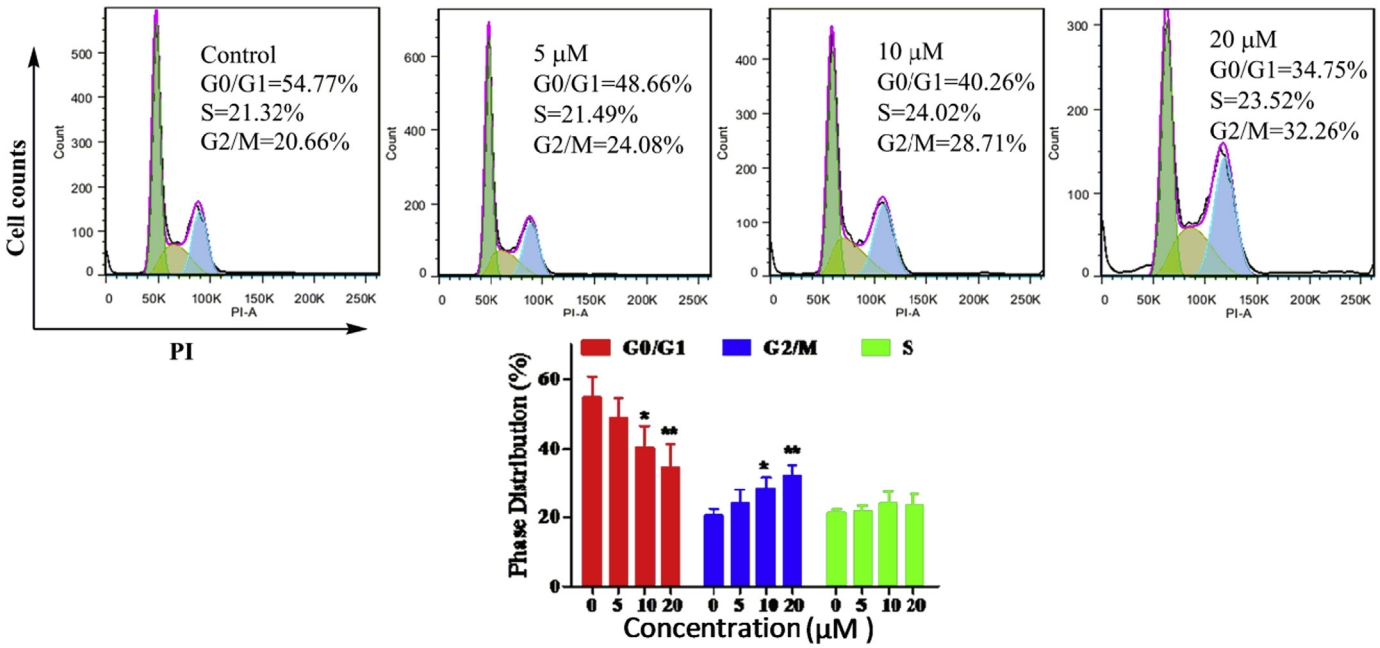


**Fig. 4.** Effect of compound **5a** on the cell cycle of MGC-803 cells. $^{*}P < 0.05$ and $^{**}P < 0.01$.

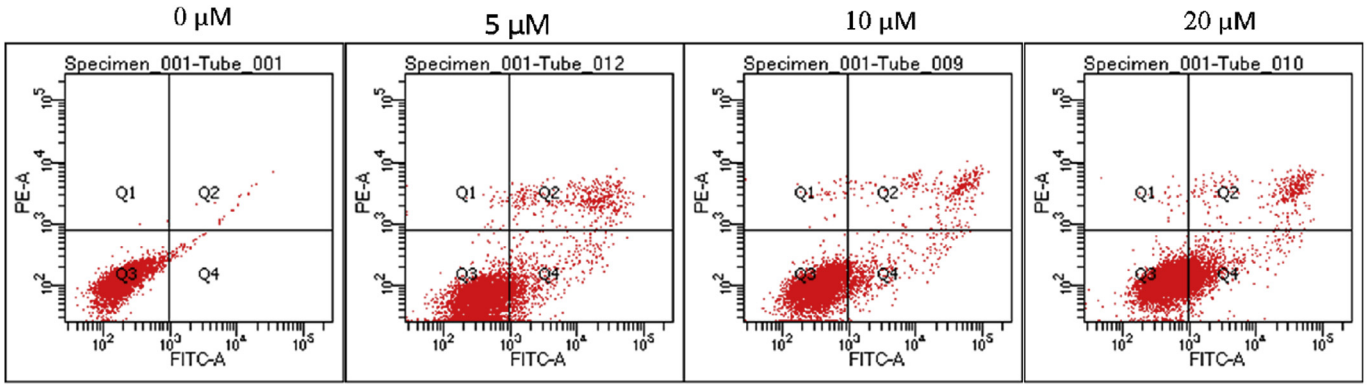


| 5a ( μ M) | 0 | 5 | 10 | 20 |
|---|---|---|---|---|
| Early apoptosis | 0.9±0.3 | 7.8±1.6 | 10.3±2.4 | 18.0±1.9 |
| Late apoptosis | 0.4±0.5 | 5.0±0.7 | 5.7±1.6 | 4.5±1.8 |

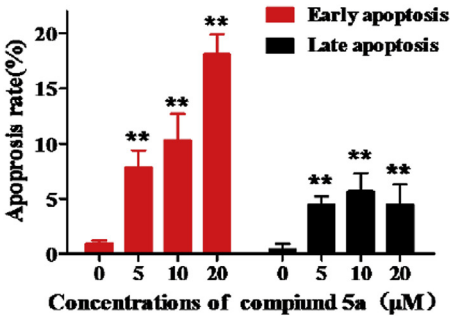


**Fig. 5.** Compound **5a** induced apoptosis of MGC-803 cells in a dose-dependent manner. $^{**}P < 0.01$.

dichlorodihydrofluorescein diacetate) assay was carried out to determine the cellular ROS levels. Principally, the non-fluorescent DCFH-DA is enzymatically hydrolyzed by cellular esterases to DCFH, followed by the ROS-mediated oxidation to form the highly fluorescent DCF [27]. The green fluorescence intensity correlates with cellular ROS levels. Therefore, the fluorescence intensity is used to reflect intracellular ROS levels. After treatment with compound **5a** at different concentrations (0, 5, 10, 20 μM), following DCFH-DA treatment for 30 min, the fluorescence intensity was analyzed using the flow cytometry. As shown in Fig. 6, compound **5a** concentration-dependently enhanced the green fluorescence intensity. The cells with green fluorescence accounted for 19.3%, significantly higher than that of the control group (2.84%).

### 2.8. Expression changes of key proteins induced by compound *5a*

It has been widely accepted that the mitochondrial dysfunction is always associated with increased ROS levels, which then induces

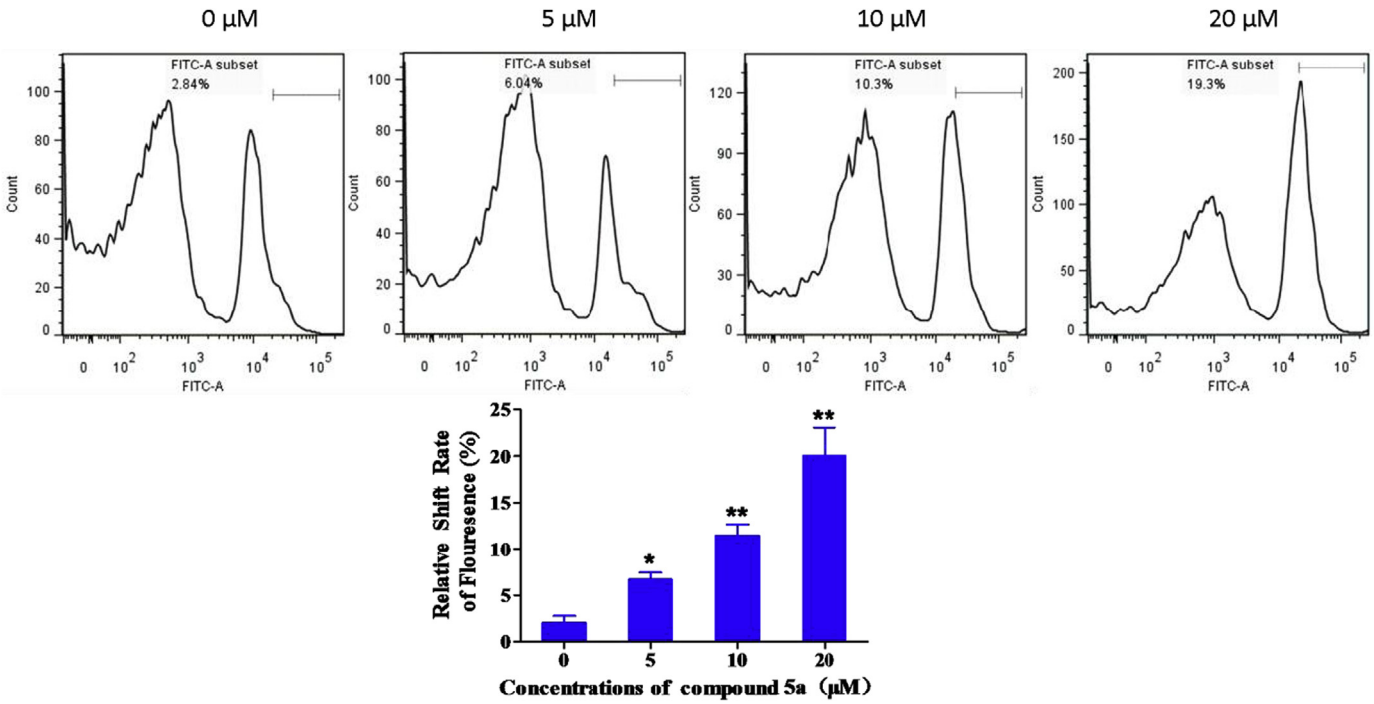


**Fig. 6.** Compound **5a** induced ROS production in MGC-803 cells. $^{*}P < 0.05$ and $^{**}P < 0.01$.

apoptosis of cancer cells through multiple mechanisms [42]. The mitochondrial dysfunction always causes the decrease of mitochondrial membrane potential, followed by release of cytochrome *c* from the mitochondria to the cytoplasm and caspase activation, finally leading to the apoptosis of cancer cells. In this study, Expression changes of key proteins were detected by the Western blot analysis. As shown in Fig. 7, compound **5a** indeed inhibited expression of LSD1 in a concentration-dependent manner, which may explain our aforementioned hypothesis that the selective inhibition of MGC-803 cells is at least in part attributed to the inactivation of LSD1. Moreover, compound **5a** activated pro-apoptotic protein Bax and inhibited expression of anti-apoptotic proteins Bcl-2 and Mcl-1. The activation of pro-apoptotic protein and inactivation of anti-apoptotic proteins finally led to the mitochondrion-mediated intrinsic apoptosis. We can also find that PARP was cleaved after compound **5a** treatment, generating the 89 kDa fragment. The cleavage of PARP is possibly attributed to the caspase activation, especially the caspase-3 and caspase-7.

Next, we further examined the expression changes of caspases by the Western blot analysis. As shown in Fig. 8, caspase-9 and caspase-8 were cleaved by compound **5a**, which then activated downstream proteins caspase-3, caspase-6 and caspase-7, finally leading to apoptosis of MGC-803 cells. Taken together, compound **5a** induced apoptosis of MGC-803 cells at least through three pathways, namely the mitochondrion-mediated intrinsic apoptotic pathway, the death receptor-mediated extrinsic apoptotic pathway, as well as the LSD1 inactivation.

### 2.9. Migration inhibition of MGC-803 cells by compound *5a*

From above studies, we can conclude that compound **5a** is capable of inducing apoptosis of MGC-803 cells through multiple mechanisms. We next investigated whether compound **5a** could inhibit migration of cancer cells. After incubation at different concentrations (0, 2, 4, 8 μM) for 24 h, MGC-803 cells were stained with Hoechst 33258, and migrated cells were detected and numbered using the high content screening system. As shown in Fig. 9, compound **5a** indeed inhibited migration of MGC-803 cells even at low concentration (2 μM), although the inhibition was not significant. Intriguingly, the inhibition was concentration-independent; the underlying mechanism remains unclear and needs to be further explored.

## 3. Conclusions

Following our previous work, we designed a series of new isatin/triazole conjugates that possessed moderate to good growth inhibition against the tested cancer cells and exerted selective inhibition against MGC-803 cells. Of these compounds, compound **5a** was the most potent one against MGC-803 cells ($IC_{50}$ = 9.78 μM) and less toxic to normal cells HL-7702 and GES-1 ($IC_{50}$ = 40.27 and 35.97 μM, respectively). Besides, compound **5a** caused morphological changes of MGC-803 cells, induced cell cycle arrest at G2/M phase, cellular ROS generation and migration inhibition of MGC-803 cells in a concentration-dependent manner. Compound **5a** induced apoptosis through the mitochondria-mediated intrinsic apoptotic pathway, the death receptor-mediated extrinsic apoptotic pathway, as well as the LSD1 inactivation. These conjugates described here may serve as bioactive fragments for developing more potent cytotoxic agents. Further modifications will focus on installation of other functional groups on the phenyl ring, replacement of triazole linker with other heterocycles, as well as further conversions based on the highly reactive C3 carbonyl group of isatin core.

## 4. Experimental section

### 4.1. General

Reagents and solvents were used directly without special treatment. Thin layer chromatography (TLC) was carried out on glass plates coated with silica gel and visualized by UV light

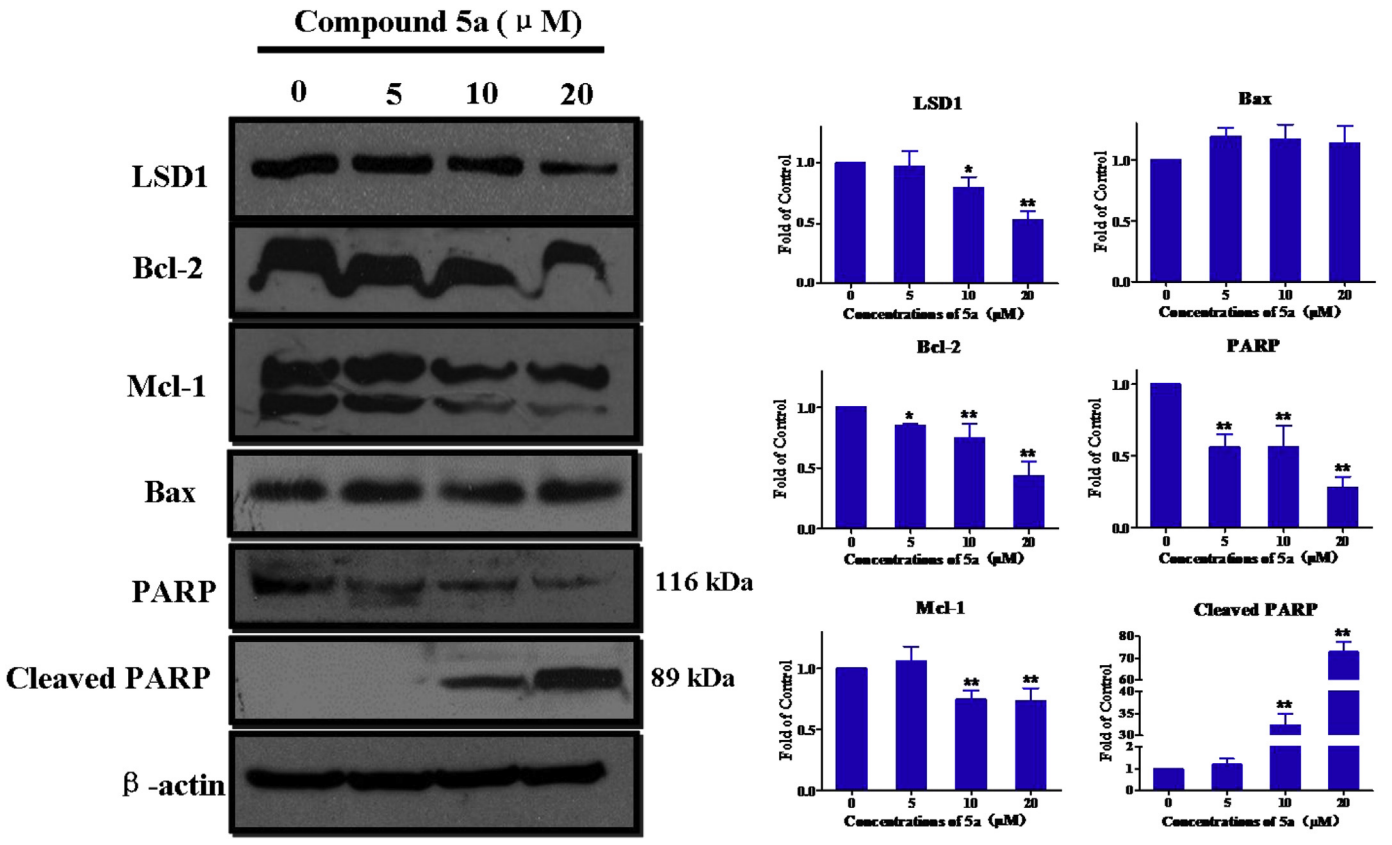


**Fig. 7.** Expression changes of key apoptotic proteins induced by compound **5a.**

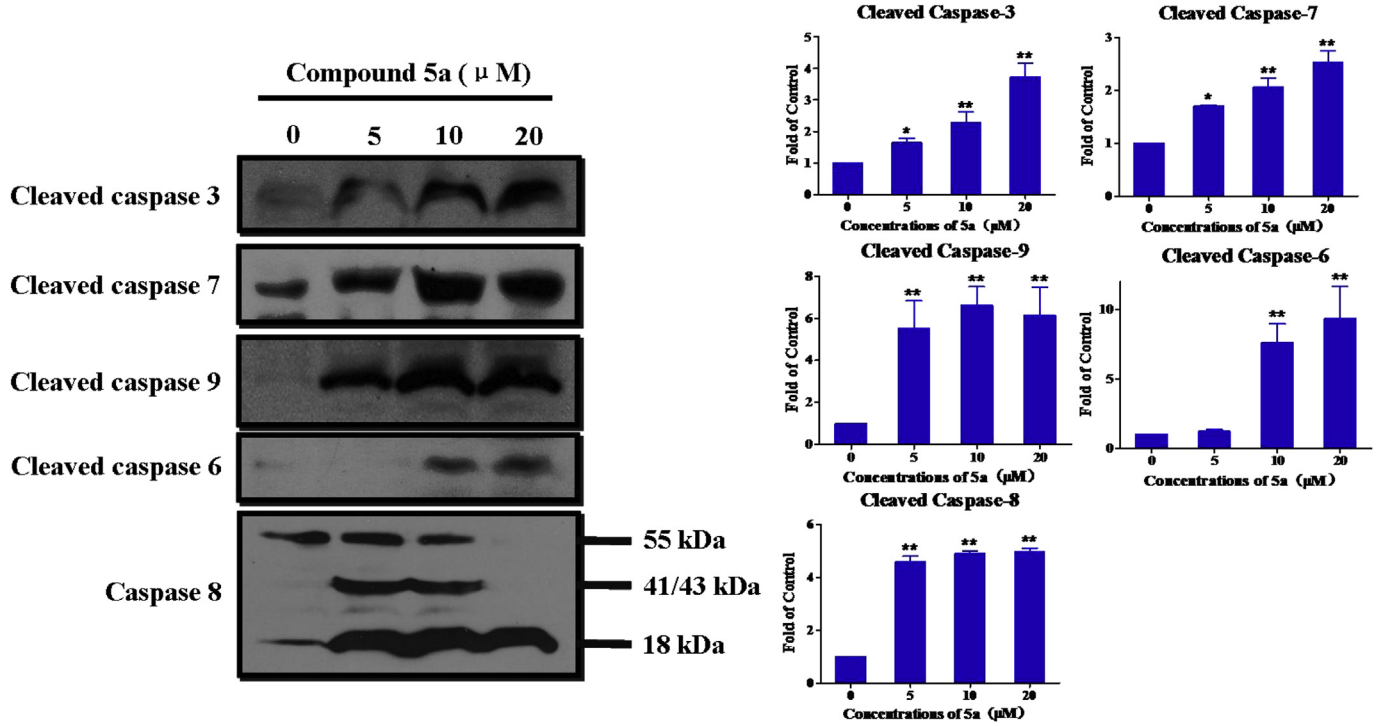


**Fig. 8.** Caspase cascade activation induced by compound **5a in MGC-803 cells**. $^{*}P < 0.05$ and $^{**}P < 0.01$.

(254 nm). Melting points were determined on an X-5 micromelting apparatus and are uncorrected. All the NMR spectra were recorded with a Bruker DPX 400 MHz spectrometer with TMS as an internal standard in $CDCl_3$ or DMSO-$d_6$. Chemical shifts are given as $\delta$ ppm

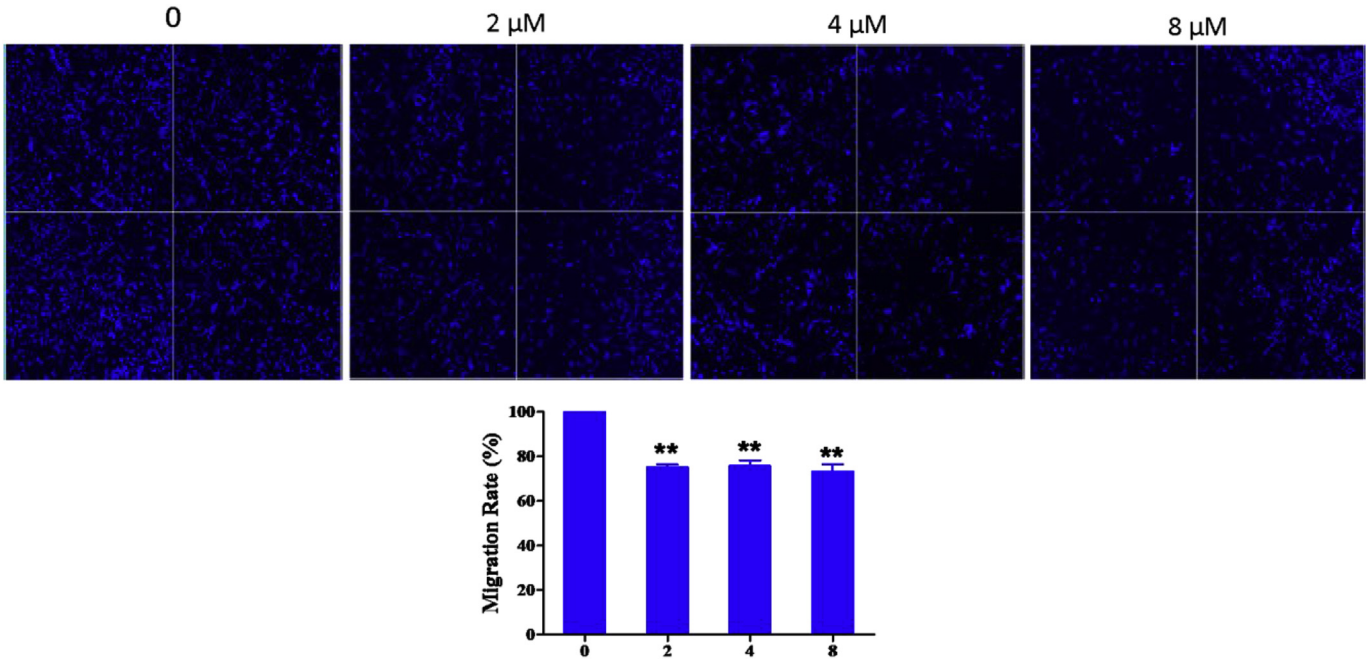


**Fig. 9.** Migration inhibition induced by compound **5a**. $^{**}P < 0.01$.

values relative to TMS. High-resolution mass spectra (HRMS) of all final compounds were recorded on a Waters Micromass Q-T of Micromass spectrometer by ESI. **CAUTION**: Particular care should be taken to avoid grinding sodium azide and acidifying mixtures containing sodium azide because the azide ion can react with acids to form the extremely explosive, volatile and toxic hydrazoic acid. Besides, sodium azide can also form highly explosive salts with many transition metals. Halogenated solvents such as dichloromethane and chloroform should be avoided for sodium azide-involved reactions and subsequent work-up procedures because such solvents can form highly explosive di- and triazidomethanes with sodium azide [43].

### 4.2. Synthesis of compound ***2***

To a solution of 4,7-dichloroisatin (0.68 mmol, 1.0 eq) in DMF (4 mL) was added $K_2CO_3$ (0.68 mmol, 1.0 eq) at room temperature, the mixture was stirred for about 30 min, and then the propargyl bromide (0.75 mmol, 1.1 eq) was added dropwise. The mixture was stirred overnight at room temperature. Upon completion, EtOAc and $H_2O$ were added. The aqueous layer was extracted with EtOAc for several times; the combined organic layers were washed with $H_2O$ for several times to remove the DMF, and then washed with brine, dried over $MgSO_4$ and evaporated to give the products. Compound **2**, saffron solid, yield: 76%, m. p.: 151.8–153.3 °C, $R_f = 0.52$ (petroleum ether/ethyl acetate = 2/1). $^1$H NMR (400 MHz, $CDCl_3$) $\delta$ 7.51 (d, $J$ = 8.7 Hz, 1H), 7.10 (d, $J$ = 8.7 Hz, 1H), 4.94 (d, $J$ = 2.4 Hz, 2H), 2.34 (t, $J$ = 2.4 Hz, 1H); $^{13}$C NMR (100 MHz, $CDCl_3$) $\delta$ 178.68, 157.00, 146.19, 140.48, 133.05, 126.79, 117.16, 116.11, 77.22, 73.27, 31.94.

### 4.3. General procedure for the synthesis of compounds ***4a–g***

To a solution of bromide **3a–g** (1.0 eq) in DMSO was added $NaN_3$ (1.2 eq) at room temperature. Then the reaction mixture was heated to 50 °C and kept for 3 h. Upon completion, EtOAc and $H_2O$ were added. The aqueous layer was extracted with EtOAc; the combined organic layers were washed with $H_2O$ for several times to remove the DMSO, and then washed with brine, dried over $MgSO_4$ and evaporated to give the corresponding products **4a–g**. Compounds **4d** and **4e** were known compounds [44] and therefore not characterized in this work.

#### 4.3.1. Compound ***4a***

Compound **4a**, light yellow liquid, 61%; $^1$H NMR (400 MHz, $CDCl_3$) $\delta$ 4.97–4.71 (m, 1H), 3.82 (s, 2H), 1.93–1.77 (m, 2H), 1.78–1.62 (m, 2H), 1.62–1.14 (m, 6H); $^{13}$C NMR (100 MHz, $CDCl_3$) $\delta$ 167.73, 74.55, 50.52, 31.43, 25.19, 23.54.

#### 4.3.2. Compound ***4b***

Compound **4b**, brown solid, yield: 55%, m.p.: 82–84 °C; $^1$H NMR (400 MHz, $CDCl_3$) $\delta$ 6.08 (s, 1H), 3.92 (s, 2H), 3.82–3.61 (m, 1H), 1.85 (m, 2H), 1.75–1.59 (m, 2H), 1.56 (m, 2H), 1.40–1.23 (m, 2H), 1.12 (m, 2H); $^{13}$C NMR (100 MHz, $CDCl_3$) $\delta$ 164.42, 51.80, 47.27, 31.95, 24.40, 23.75.

#### 4.3.3. Compound ***4c***

Compound **4c**, white solid, yield: 63%, m.p.: 83–86 °C; $^1$H NMR (400 MHz, $CDCl_3$) $\delta$ 7.94 (s, 1H), 7.47 (d, $J$ = 7.7 Hz, 2H), 7.29 (dd, $J$ = 10.8, 5.1 Hz, 2H), 7.09 (t, $J$ = 7.4 Hz, 1H), 4.08 (s, 2H); $^{13}$C NMR (100 MHz, $CDCl_3$) $\delta$ 163.45, 135.70, 128.12, 124.05, 119.03, 51.99.

#### 4.3.4. Compound ***4f***

Compound **4f**, light yellow solid, yield: 11%, m.p.: 69–71 °C; $^1$H NMR (400 MHz, $CDCl_3$) $\delta$ 3.94 (s, 2H), 3.70 (t, $J$ = 4.8 Hz, 4H), 3.66 (d, $J$ = 5.1 Hz, 2H), 3.43–3.36 (m, 2H); $^{13}$C NMR (100 MHz, $CDCl_3$) $\delta$ 164.76, 65.75, 65.42, 49.61, 44.53, 41.29.

#### 4.3.5. Compound ***4g***

Compound **4g**, white solid, yield: 74%, m.p.: 118–120 °C; $^1$H NMR (400 MHz, $CDCl_3$) $\delta$ 3.88 (s, 2H), 3.55 (d, $J$ = 5.2 Hz, 2H), 3.39 (s, 4H), 3.30 (d, $J$ = 5.2 Hz, 2H), 1.41 (s, 9H); $^{13}$C NMR (100 MHz, $CDCl_3$) $\delta$ 164.78, 153.85, 153.41, 79.55, 49.79, 43.99, 40.86, 27.33.

### 4.4. General procedure for the synthesis of compounds **5a–g**

To a solution of azide (1.0 eq) and alkyne (1.0 eq) in THF/$H_2O$ (1/1) were added soduim ascorbate (0.5 eq) and $CuSO_4 \cdot 5H_2O$ (0.4 eq) at room temperature. The mixture was then stirred for 5–8 h at room temperature. Upon completion, the mixture was filtered and washed with $H_2O$ to give the products.

#### 4.4.1. Compound **5a**

Compound **5a**, yellow solid, yield: 50%, m. p.: 163.1–164.7 °C, $R_f = 0.25$ (PE/acetone = 2/1); $^1$H NMR (400 MHz, DMSO-$d_6$) $\delta$ 8.18 (s, 1H), 7.62 (d, $J = 8.7$ Hz, 1H), 7.19 (d, $J = 8.7$ Hz, 1H), 5.34 (s, 2H), 5.31 (s, 2H), 4.81–4.63 (m, 1H), 1.78–1.65 (m, 2H), 1.57 (m, 2H), 1.49–1.11 (m, 6H); $^{13}$C NMR (100 MHz, DMSO-$d_6$) $\delta$ 178.54, 166.33, 158.05, 146.30, 142.96, 139.73, 130.21, 125.63, 124.30, 117.50, 114.55, 73.43, 50.52, 37.35, 30.64, 24.60, 22.67; HRMS (ESI): $m/z$ calcd for $C_{19}H_{18}Cl_2N_4NaO_4$ $(M + Na)^+$, 459.0603; found, 459.0599.

#### 4.4.2. Compound **5b**

Compound **5b**, orange solid, yield: 84%, m. p.: 269.3–270.5 °C, $R_f = 0.53$ (PE/acetone = 1/1); $^1$H NMR (400 MHz, DMSO-$d_6$) $\delta$ 8.22 (d, $J = 7.5$ Hz, 1H), 8.12 (s, 1H), 7.62 (d, $J = 8.7$ Hz, 1H), 7.19 (d, $J = 8.7$ Hz, 1H), 5.29 (s, 2H), 5.00 (s, 2H), 3.57–3.41 (m, 1H), 1.69 (m, 4H), 1.53 (m, 1H), 1.41–0.99 (m, 5H). $^{13}$C NMR (100 MHz, DMSO-$d_6$) $\delta$ 178.65, 164.05, 158.16, 146.45, 142.72, 139.81, 130.27, 125.68, 124.37, 117.58, 114.64, 51.72, 47.77, 37.48, 32.19, 25.08, 24.31; HRMS (ESI): $m/z$ calcd for $C_{19}H_{20}Cl_2N_5O_3$ $(M + H)^+$, 436.0943; found, 436.0945.

#### 4.4.3. Compound **5c**

Compound **5c**, yellow solid, yield: 64%, m. p.: 213.6–214.9 °C, $R_f = 0.10$ (PE/acetone = 2/1); $^1$H NMR (400 MHz, DMSO-$d_6$) $\delta$ 10.45 (s, 1H), 8.21 (s, 1H), 7.63 (d, $J = 8.7$ Hz, 1H), 7.56 (d, $J = 7.9$ Hz, 2H), 7.32 (t, $J = 7.7$ Hz, 2H), 7.19 (d, $J = 8.7$ Hz, 1H), 7.08 (t, $J = 7.3$ Hz, 1H), 5.32 (s, 2H), 5.29 (s, 2H); $^{13}$C NMR (100 MHz, DMSO-$d_6$) $\delta$ 178.64, 164.04, 158.17, 146.46, 139.83, 138.33, 130.29, 128.87, 125.70, 123.76, 119.17, 117.58, 114.65, 52.27, 37.50; HRMS (ESI): $m/z$ calcd for $C_{19}H_{14}Cl_2N_5O_3$ $(M + H)^+$, 430.0474; found, 430.0470.

#### 4.4.4. Compound **5d**

Compound **5d**, orange solid, yield: 63%, m. p.: 205.6–206.8 °C, $R_f = 0.09$ (PE/acetone = 2/1); $^1$H NMR (400 MHz, DMSO-$d_6$) $\delta$ 8.08 (s, 1H), 7.62 (d, $J = 8.7$ Hz, 1H), 7.19 (d, $J = 8.7$ Hz, 1H), 5.39 (s, 2H), 5.30 (s, 2H), 3.40 (s, 4H), 1.54 (d, $J = 24.8$ Hz, 4H), 1.42 (s, 2H); $^{13}$C NMR (100 MHz, DMSO-$d_6$) $\delta$ 178.65, 163.62, 158.14, 146.44, 139.80, 130.27, 125.69, 124.61, 117.60, 114.64, 50.74, 45.19, 42.42, 37.52, 25.72, 25.10, 23.76; HRMS (ESI): $m/z$ calcd for $C_{18}H_{18}Cl_2N_5O_3$ $(M + H)^+$, 422.0787; found, 422.0784.

#### 4.4.5. Compound **5e**

Compound **5e**, yellow solid, yield: 53%, m. p.: 221.0–226.7 °C, $R_f = 0.28$ (PE/acetone = 1/1); $^1$H NMR (400 MHz, DMSO-$d_6$) $\delta$ 8.08 (s, 1H), 7.62 (d, $J = 8.7$ Hz, 1H), 7.19 (d, $J = 8.7$ Hz, 1H), 5.30 (s, 4H), 3.48 (t, $J = 6.7$ Hz, 2H), 3.29 (t, $J = 6.8$ Hz, 2H), 1.89 (quintet, $J = 13.3$, 6.6 Hz, 2H), 1.78 (quintet, $J = 13.3$, 6.7 Hz, 2H); $^{13}$C NMR (100 MHz, DMSO-$d_6$) $\delta$ 178.65, 163.60, 158.16, 146.46, 139.81, 130.28, 125.69, 124.48, 117.59, 114.66, 51.27, 45.75, 45.06, 37.50, 25.52, 23.67; HRMS (ESI): $m/z$ calcd for $C_{17}H_{15}Cl_2N_5NaO_3$ $(M+Na)^+$, 430.0450; found, 430.0451.

#### 4.4.6. Compound **5f**

Compound **5f**, yellow solid, yield: 58%, m. p.: 205.7–207.0 °C, $R_f = 0.25$ (PE/acetone = 1/1); $^1$H NMR (400 MHz, DMSO-$d_6$) $\delta$ 8.08 (s, 1H), 7.62 (d, $J = 8.7$ Hz, 1H), 7.19 (d, $J = 8.7$ Hz, 1H), 5.43 (s, 2H), 5.33 (s, 2H), 3.61 (s, 2H), 3.55 (s, 2H), 3.48 (s, 2H), 3.42 (s, 2H); $^{13}$C NMR (100 MHz, DMSO-$d_6$) $\delta$ 178.65, 164.32, 158.15, 146.44, 139.81, 130.28, 125.70, 117.60, 114.64, 65.90, 65.81, 50.59, 44.71, 41.85, 37.52.; HRMS (ESI): $m/z$ calcd for $C_{17}H_{16}Cl_2N_5O_4$ $(M+H)^+$, 424.0579; found, 424.0582.

#### 4.4.7. Compound **5g**

Compound **5g**, yellow solid, yield: 73%, m. p.: 203.1–204.4 °C, $R_f = 0.09$ (PE/acetone = 2/1); $^1$H NMR (400 MHz, DMSO-$d_6$) $\delta$ 8.08 (s, 1H), 7.61 (d, $J = 8.7$ Hz, 1H), 7.19 (d, $J = 8.7$ Hz, 1H), 5.45 (s, 2H), 5.30 (s, 2H), 3.66–3.35 (m, 8H), 1.41 (s, 9H); $^{13}$C NMR (100 MHz, DMSO-$d_6$) $\delta$ 178.64, 164.31, 158.15, 153.73, 146.44, 139.80, 130.28, 125.70, 117.60, 114.64, 79.22, 50.70, 43.97, 41.30, 37.51, 27.99; HRMS (ESI): $m/z$ calcd for $C_{22}H_{24}Cl_2N_6NaO_5$ $(M+Na)^+$, 545.1083; found, 545.1069.

### 4.5. Synthesis of compound **5h**

Compound **5g** (30 mg, 0.057 mmol, 1.0 eq) was dissolved in DCM (2 mL), followed by addition of TFA (166.8 mg, 1.72 mmol, 30 eq). The resulting solution was kept at rt for 2 h. Then the mixture was diluted with DCM. The organic phase was washed with saturated $Na_2CO_3$ and $H_2O$ twice, drived over $MgSO_4$ and evaporated under vacuum to give compound **5h**. Orange-red solid, yield: 31%, m.p.: 138.1–139.5 °C, $R_f = 0.16$ (DCM/MeOH = 2/1); $^1$H NMR (400 MHz, DMSO-$d_6$) $\delta$ 8.98 (brs, 2H), 8.05 (s, 1H), 7.62 (d, $J = 8.7$ Hz, 1H), 7.19 (d, $J = 8.7$ Hz, 1H), 5.49 (s, 2H), 5.31 (s, 2H), 3.92–3.09 (m, 8H); $^{13}$C NMR (100 MHz, DMSO-$d_6$) $\delta$ 178.64, 164.50, 158.17, 146.44, 139.82, 130.30, 125.71, 124.62, 117.58, 114.64, 50.53, 42.50, 41.32, 38.38, 37.48; HRMS (ESI): $m/z$ calcd for $C_{17}H_{17}Cl_2N_6O_3$ $(M+H)^+$, 423.0734; found, 423.0737.

### 4.6. Cytotoxic evaluation

All the human carcinoma cell lines were purchased from the Cell Bank of the Chinese Academy of Science (Shanghai, China) and cultured in at 37 °C in a humidified atmosphere containing 5% $CO_2$. The CCK-8 method was used to investigate the cytotoxicity of synthesized compounds against human breast, bladder, esophageal and gastric cancer cell lines (MCF-7, SW-780, TE-1 and MGC-803) and two normal cells (HL-702 and GES-1). In brief, cells were collected during the exponential growth phase following trypsinization. 100 μL Cells suspension ($2 \times 10^4$ cells/mL) were seeded in 96-well plates culture medium each well. After 24 h' incubation, the medium was removed and replaced by 200 μL medium containing different concentrations of compounds mentioned above (0.5, 1, 2, 4, 8, 16, 32, 64, 128, 256 μM). The control wells were added with fresh medium. The plates were incubated at 37 °C in 5% $CO_2$ for 72 h. Thereafter, the cells were cultured for 4 h at 37 °C with 7 μL of CCK-8 in each well. The mixture was shaken for 10 min at room temperature. The absorbance was measured using a microplate reader (BioTek Instruments, Inc., VT) at 450 nm. All experiments were performed three times. $IC_{50}$ values were calculated by software SPSS 20.0 and showed by mean and SD.

### 4.7. Hoechst 33258 staining assay

Cells were seeded on glass slides placed in 24-well plates. After growing to approximately 70% confluence, the cells were treated with 0, 5, 10 and 20 μM of compound **5a** for 24 h. Then cells were washed with PBS for three times, and incubated with Hoechst 33258 staining buffer (10 μg/mL Hoechst 3325 and 0.1% Triton X-100) in dark for 20 min. Then cells were washed with PBS three times, the slides seeded with the cells were mounted and analyzed by Laser Scanning Confocal Microscope (Nikon A1R, Tokyo, Japan).

### 4.8. Cell cycle distribution assay by flow cytometry

Cells were seeded in 6-well plates and treated with 0, 5, 10 and 20 μM of compound **5a** for 24 h. Then cells were collected and fixed by 70% ethanol at 4 °C overnight. The fixed cells were washed with cold PBS and resuspended in 100 ul PBS containing 10 μg/mL RNase A and 50 μg/mL PI for 20 min in dark. Samples were then analyzed for DNA content by flow cytometry (Becton, Dickinson and Company, NJ.).

### 4.9. Apoptosis detection by flow cytometry

An Annexin V-FITC/PI kit (KeyGEN BioTECH, Nanjing, China) was used to detect apoptosis. Cells were seeded in 6-well plates and treated with 0, 5, 10 and 20 μM of compound **5a** for 24 h. Then the cells were collected and suspended in binding buffer containing Annexin V-FITC (0.5 mg/mL) and PI (0.5 mg/mL) and incubated in dark for 20 min and analyzed by flow cytometry (Becton, Dickinson and Company, NJ).

### 4.10. Measurement of intracellular ROS levels

The redox-sensitive probe 2,7-dichlorodihydrofluorescein diacetate was used to measure intracellular ROS levels. Cells were seeded and treated with 0, 5, 10, and 20 μM of compound **5a** for 24 h, then cells were collected and incubated with DCFH-DA (10 μM) for 30 min at 37 °C. Then cells were washed with serum free medium for three times. And the fluorescence intensity was determined by a flow cytometer.

### 4.11. Western blot analysis

Cells were seeded and treated with 0, 5,10 and 20 μM of compound **5a** for 24 h, then cells were collected and lysed by radio immunoprecipitation assay (RIPA) lysis buffer (50 mM Tris-HCl, pH 7.5, 150 mM NaCl, 0.25% sodium deoxycholate, 0.1% Nonidet P-40, 0.1% Triton X-100) with the complete proteinase inhibitor cocktail (Roche, Basel, Switzerland) for 30 min. After centrifugation of 12,000 rpm for 10 min at 4 °C, supernatant was collected and the protein concentration was detected using a bicinchonininc acid (BCA) assay kit (Beyotmie Biotechnology, Haimen, China). After added with loading buffer, cell lyses were boiled for 10 min at 100 °C for SDS-polyacrylamide gel electrophoresis (PAGE). Proteins were transferred to nitrocellulose (NC) membranes. The membranes were blocked with 5% skim milk at room temperature for 2 h, and then incubated overnight at 4 °C with primary antibodies. After washing the membrane with TBST (TBS, 0.05% Tween-20)/TBS three times (5 min per wash), blots were incubated with the secondary antibody (1:5000) at room temperature for 2 h. Finally, the blots were washed in TBST/TBS. The antibody-reactive bands were revealed by enhanced chemiluminescence (ECL) and exposed on Kodak radiographic film.

### 4.12. Transwell assay

For the migration assay, 100 μL medium containing 1% FBS, different concentrations of compound **5a** and 10, 000 cells were added to each upper chamber. In the lower chamber, 500 μL medium with 20% FBS was used as chemoattractant. After incubation for 24 h, both chambers were washed by PBS for three times. After staining with Hoechst 33258 (10 μg/mL) and twice wash, migrated cells were detected and numbered using high content screening system (ArrayScan XTI, Thermo Fisher Scientific, MA).

### 4.13. Statistical analysis

Data are presented as mean ± SD from three independent experiments. SPSS statistics version 20.0 (IBM, New York City, NY) was used to calculate $IC_{50}$ and one-way ANOVA was employed to determine statistical significance using GraphPad Prism 5 (GraphPad Software Inc., San Diego, CA). $^{*}P < 0.05$, $^{**}P < 0.01$, as compared with the control group.

## Acknowledgment

We gratefully acknowledge the National Natural Science Foundation of China (No. 21372206) and the Development Foundation of Priority, Ministry of Education (No. 20134101130001) for the financial support. Bin Yu is grateful for the financial support from the Outstanding PhD Training Program of Zhengzhou University.

## Appendix A. Supplementary data

Supplementary data related to this article can be found at http://dx.doi.org/10.1016/j.ejmech.2016.08.065.

## References

[1] M. d'Ischia, A. Palumbo, G. Prota, Adrenalin oxidation revisited. New products beyond the adrenochrome stage, Tetrahedron 44 (1988) 6441–6446.
[2] J. Song, L. Hou, C. Ju, J. Zhang, Y. Ge, W. Yue, Isatin inhibits proliferation and induces apoptosis of SH-SY5Y neuroblastoma cells *in vitro* and *in vivo*, Eur. J. Pharmacol. 702 (2013) 235–241.
[3] L. Hou, C. Ju, J. Zhang, J. Song, Y. Ge, W. Yue, Antitumor effects of isatin on human neuroblastoma cell line (SH-SY5Y) and the related mechanism, Eur. J. Pharmacol. 589 (2008) 27–31.
[4] X. Jiang, Y. Sun, J. Yao, Y. Cao, M. Kai, N. He, X. Zhang, Y. Wang, R. Wang, Core scaffold-inspired concise synthesis of chiral spirooxindole-pyranopyrimidines with broad-spectrum anticancer potency, Adv. Synth. Catal. 354 (2012) 917–925.
[5] L. Hong, R. Wang, Recent advances in asymmetric organocatalytic construction of 3,3′-Spirocyclic oxindoles, Adv. Synth. Catal. 355 (2013) 1023–1052.
[6] B. Yu, D.Q. Yu, H.M. Liu, Spirooxindoles: promising scaffolds for anticancer agents, Eur. J. Med. Chem. 97 (2015) 673–698.
[7] Z. Zhang, X.J. Chu, J.J. Liu, Q. Ding, J. Zhang, D. Bartkovitz, N. Jiang, P. Karnachi, S.S. So, C. Tovar, Z.M. Filipovic, B. Higgins, K. Glenn, K. Packman, L. Vassilev, B. Graves, Discovery of potent and orally active p53-MDM2 inhibitors RO5353 and RO2468 for potential clinical development, ACS Med. Chem. Lett. 5 (2013) 124–127.
[8] B. Yu, Y.C. Zheng, X.J. Shi, P.P. Qi, H.M. Liu, Natural product-derived spirooxindole fragments serve as privileged substructures for discovery of new anticancer agents, Anticancer Agents Med. Chem. (2016), http://dx.doi.org/10.2174/1871520615666151102093825.
[9] C.V. Galliford, K.A. Scheidt, Pyrrolidinyl-spirooxindole natural products as inspirations for the development of potential therapeutic agents, Angew. Chem. Int. Ed. 46 (2007) 8748–8758.
[10] S. Wang, W. Sun, Y. Zhao, D. McEachern, I. Meaux, C. Barrière, J.A. Stuckey, J.L. Meagher, L. Bai, L. Liu, C.G. Hoffman-Luca, J. Lu, S. Shangary, S. Yu, D. Bernard, A. Aguilar, O. Dos-Santos, L. Besret, S. Guerif, P. Pannier, D. Gorge-Bernat, L. Debussche, SAR405838: an optimized inhibitor of MDM2–p53 interaction that induces complete and durable tumor regression, Cancer Res. 74 (2014) 5855–5865.
[11] B. Yu, Z. Yu, P.P. Qi, D.Q. Yu, H.M. Liu, Discovery of orally active anticancer candidate CFI-400945 derived from biologically promising spirooxindoles: success and challenges, Eur. J. Med. Chem. 95 (2015) 35–40.
[12] N.J. White, S. Pukrittayakamee, A.P. Phyo, R. Rueangweerayut, F. Nosten, P. Jittamala, A. Jeeyapant, J.P. Jain, G. Lefèvre, R. Li, B. Magnusson, T.T. Diagana, F.J. Leong, Spiroindolone KAE609 for falciparum and vivax malaria, N. Engl. J. Med. 371 (2014) 403–410.
[13] G.S. Singh, Z.Y. Desta, Isatins as privileged molecules in design and synthesis of spiro-fused cyclic frameworks, Chem. Rev. 112 (2012) 6104–6155.
[14] N.R. Ball-Jones, J.J. Badillo, A.K. Franz, Strategies for the enantioselective synthesis of spirooxindoles, Org. Biomol. Chem. 10 (2012) 5165–5181.
[15] M. Xia, R.Z. Ma, Recent progress on routes to spirooxindole systems derived from isatin, J. Heterocycl. Chem. 51 (2013) 539–554.
[16] S.G. Agalave, S.R. Maujan, V.S. Pore, Click chemistry: 1,2,3-Triazoles as pharmacophores, Chem. Asian J. 6 (2011) 2696–2718.
[17] A. Massarotti, S. Aprile, V. Mercalli, E. Del Grosso, G. Grosa, G. Sorba, G.C. Tron, Are 1,4- and 1,5-Disubstituted 1,2,3-Triazoles good pharmacophoric groups? ChemMedChem 9 (2014) 2497–2508.
[18] D. González-Calderón, M.G. Mejía-Dionicio, M.A. Morales-Reza, A. Ramírez-

Villalva, M. Morales-Rodríguez, B. Jauregui-Rodríguez, E. Díaz-Torres, C. González-Romero, A. Fuentes-Benítes, Azide-enolate 1,3-dipolar cycloaddition in the synthesis of novel triazole-based miconazole analogues as promising antifungal agents, Eur. J. Med. Chem. 112 (2016) 60–65.
[19] B. Yu, X.J. Shi, P.P. Qi, D.Q. Yu, H.M. Liu, Design, synthesis and biological evaluation of novel steroidal spiro-oxindoles as potent antiproliferative agents, J. Steroid Biochem. Mol. Biol. 141 (2014) 121–134.
[20] B. Yu, P.P. Qi, X.J. Shi, L.H. Shan, D.Q. Yu, H.M. Liu, Discovery of novel steroidal pyran–oxindole hybrids as cytotoxic agents, Steroids 88 (2014) 44–52.
[21] B. Yu, X.N. Sun, X.J. Shi, P.P. Qi, Y.C. Zheng, D.Q. Yu, H.M. Liu, Efficient synthesis of novel antiproliferative steroidal spirooxindoles via the [3+2] cycloaddition reactions of azomethine ylides, Steroids 102 (2015) 92–100.
[22] Y.L. Zhang, Y.F. Li, J.W. Wang, B. Yu, Y.K. Shi, H.M. Liu, Multicomponent assembly of novel antiproliferative steroidal dihydropyridinyl spirooxindoles, Steroids 109 (2016) 22–28.
[23] B. Yu, P.P. Qi, X.J. Shi, R. Huang, H. Guo, Y.C. Zheng, D.Q. Yu, H.M. Liu, Efficient synthesis of new antiproliferative steroidal hybrids using the molecular hybridization approach, Eur. J. Med. Chem. 117 (2016) 241–255.
[24] Y.H. Yang, H. Aloysius, D. Inoyama, Y. Chen, L.Q. Hu, Enzyme-mediated hydrolytic activation of prodrugs, Acta Pharm. Sin. B 1 (2011) 143–159.
[25] J. Rautio, H. Kumpulainen, T. Heimbach, R. Oliyai, D. Oh, T. Jarvinen, J. Savolainen, Prodrugs: design and clinical applications, Nat. Rev. Drug Discov. 7 (2008) 255–270.
[26] P. Huang, D. Wang, Y. Su, W. Huang, Y. Zhou, D. Cui, X. Zhu, D. Yan, Combination of small molecule prodrug and nanodrug delivery: amphiphilic drug–drug conjugate for Cancer therapy, J. Am. Chem. Soc. 136 (2014) 11748–11756.
[27] R.P. Rastogi, S.P. Singh, D.P. Häder, R.P. Sinha, Detection of reactive oxygen species (ROS) by the oxidant-sensing probe 2′,7′-dichlorodihydrofluorescein diacetate in the cyanobacterium Anabaena variabilis PCC 7937, Biochem. Biophys. Res. Commun. 397 (2010) 603–607.
[28] S. Schulz, J.W. Nyce, Inhibition of protein isoprenylation and p21ras membrane association by dehydroepiandrosterone in human colonic adenocarcinoma cells *in vitro*, Cancer Res. 51 (1991) 6563–6567.
[29] R. Vegliante, E. Desideri, L. Di Leo, M.R. Ciriolo, Dehydroepiandrosterone triggers autophagic cell death in human hepatoma cell line HepG2 via JNK-mediated p62/SQSTM1 expression, Carcinogenesis 37 (2016) 233–244.
[30] Clinical development plan: dehydroepiandrosterone (DHEA), J. Cell. Biochem. 63 (1996) 86–99.
[31] A.G. Schwartz, L. Pashko, J.M. Whitcomb, Inhibition of tumor development by dehydroepiandrosterone and related steroids, Toxicol. Pathol. 14 (1986) 357–362.
[32] D. Safiulina, N. Peet, E. Seppet, A. Zharkovsky, A. Kaasik, Dehydroepiandrosterone inhibits complex I of the mitochondrial respiratory chain and is neurotoxic *in vitro* and *in vivo* at high concentrations, Toxicol. Sci. 93 (2006) 348–356.
[33] X.W. Ye, Y.C. Zheng, Y.C. Duan, M.M. Wang, B. Yu, J.L. Ren, J.L. Ma, E. Zhang, H.M. Liu, Synthesis and biological evaluation of coumarin-1,2,3-triazole-dithiocarbamate hybrids as potent LSD1 inhibitors, MedChemComm 5 (2014) 650–654.
[34] Y.C. Zheng, Y.C. Duan, J.L. Ma, R.M. Xu, X. Zi, W.L. Lv, M.-M. Wang, X.W. Ye, S. Zhu, D. Mobley, Y.Y. Zhu, J.W. Wang, J.F. Li, Z.R. Wang, W. Zhao, H.M. Liu, Triazole-Dithiocarbamate based selective lysine specific demethylase 1 (LSD1) inactivators inhibit gastric Cancer cell growth, invasion, and migration, J. Med. Chem. 56 (2013) 8543–8560.
[35] L.Y. Ma, Y.C. Zheng, S.Q. Wang, B. Wang, Z.R. Wang, L.P. Pang, M. Zhang, J.W. Wang, L. Ding, J. Li, C. Wang, B. Hu, Y. Liu, X.D. Zhang, J.J. Wang, Z.J. Wang, W. Zhao, H.M. Liu, Design, synthesis, and structure-activity relationship of novel LSD1 inhibitors based on pyrimidine-thiourea hybrids as potent, orally active antitumor agents, J. Med. Chem. 58 (2015) 1705–1716.
[36] C.A. Lipinski, F. Lombardo, B.W. Dominy, P.J. Feeney, Experimental and computational approaches to estimate solubility and permeability in drug discovery and development settings, Adv. Drug Deliv. Rev. 46 (2001) 3–26.
[37] E. Ginsburg, D. Salomon, T. Sreevalsan, E. Freese, Growth inhibition and morphological changes caused by lipophilic acids in mammalian cells, Proc. Natl. Acad. Sci. U. S. A. 70 (1973) 2457–2461.
[38] Alexi I. Goranov, A. Gulati, N. Dephoure, T. Takahara, T. Maeda, Steven P. Gygi, S. Manalis, A. Amon, Changes in cell morphology are coordinated with cell growth through the TORC1 pathway, Curr. Biol. 23 (2013) 1269–1279.
[39] G.K. Schwartz, M.A. Shah, Targeting the cell cycle: a new approach to Cancer therapy, J. Clin. Oncol. 23 (2005) 9408–9421.
[40] L.Z. de Oliveira, I.L.G. Farias, M. Rigo, W.G. Glanzner, P.B.D. Goncalves, F.C. Cadona, I.B. Cruz, J.G. Farias, M.M.M.F. Duarte, L. Franco, G. Bertol, E. Colpo, P.C. Brites, J.B.T. Rocha, D.B.R. Leal, Effect of Uncaria tomentosa extract on apoptosis triggered by oxaliplatin exposure on HT29 cells, Evid. Based Complement. Altern. Med. 2014 (2014) 1–10.
[41] K.R. Senwar, P. Sharma, T.S. Reddy, M.K. Jeengar, V.L. Nayak, V.G.M. Naidu, A. Kamal, N. Shankaraiah, Spirooxindole-derived morpholine-fused-1,2,3-triazoles: design, synthesis, cytotoxicity and apoptosis inducing studies, Eur. J. Med. Chem. 102 (2015) 413–424.
[42] Y.H. Han, Y.M. Yang, S.Z. Kim, W.H. Park, Attenuation of MG132-induced HeLa cell death by N-Acetyl cysteine via reducing reactive oxygen species and preventing glutathione depletion, Anticancer Res. 30 (2010) 2107–2112.
[43] F. González-Bobes, N. Kopp, L. Li, J. Deerberg, P. Sharma, S. Leung, M. Davies, J. Bush, J. Hamm, M. Hrytsak, Scale-up of azide chemistry: a case study, Org. Process Res. Dev. 16 (2012) 2051–2057.
[44] D. Lee, D. Kim, S. Lee, T. Kim, J. Kim, S. Kim, K.H. Liu, S. Lee, J.S. Bae, K.S. Song, C.W. Cho, Y.K. Son, D.J. Baek, T. Lee, Efficient syntheses of 1,2,3-Triazoloamide derivatives using solid-and solution-phase synthetic approaches, Molecules 20 (2015) 19984–20013.